JOURNAL OF MAGNETIC RESONANCE **125,** 340–347 (1997)
ARTICLE NO. MN971125

RF Gradient BIRD/TANGO Sequence to Eliminate Uncoupled Magnetization

AARON SODICKSON* AND DAVID G. CORY †,‡

*Harvard–MIT Division of Health Sciences and Technology; and †Department of Nuclear Engineering, Massachusetts Institute of Technology, Cambridge, Massachusetts 02139

Received December 27, 1996

A modification of the BIRD and TANGO sequences is presented which employs radiofrequency field gradients to eliminate the net magnetization from uncoupled spins, while completely preserving coupled magnetization. The standard BIRD and TANGO sequences cause selective nutation of protons directly bound to a coupling partner, while returning uncoupled magnetization to $+z$. These sequences lend themselves naturally to modification using RF gradients, which require no increase in pulse-sequence complexity while providing substantial suppression of uncoupled resonances and elimination of typical antiphase and multiple-quantum error terms that arise from improperly set pulse lengths or delays. In the RF-gradient BIRD/TANGO sequence, the uncoupled magnetization is dephased in a plane orthogonal to the RF axis, while the desired signal components are refocused, effectively in a rotary echo. The sequence has applications to solvent suppression and selective isotopomer excitation. It is demonstrated for selective excitation of the satellites in a sample of chloroform, yielding suppression of the uncoupled magnetization by a factor of approximately 800.

INTRODUCTION

Ubiquitous in NMR spectroscopy is the need to study a particular signal of interest in the presence of background signals that may be comparatively quite large. A number of techniques exist to remove the unwanted signal components. The most widely used of these techniques rely on phase cycling or on the application of B_0 gradients. Phase cycling relies on systematically changing RF phases in the pulse cycle to alter the phases of signal components during subsequent scans. The resulting signals are then combined in such a way that the desired signal adds constructively while undesired components cancel to zero. This, however, requires numerous acquisitions and yields poor digitizer resolution for small signals of interest, as the digitizer dynamic range is filled in each scan by the dominant unwanted resonances (e.g., the solvent signal) before being removed by signal combination.

Static B_0 gradient techniques (*1*) are commonly used with a similar rationale. Gradient pulses are applied at appropriate points in the pulse cycle and produce a spatially dependent phase evolution in the various coherences present. By choosing appropriate gradient pulse lengths and timings, one can arrange for part of the desired signal to pass through the pulse sequence in phase, while unwanted signal components are left with a spatially dependent phase factor that causes the net signal to integrate to zero over the full sample volume. B_0 gradient techniques have the advantage that unwanted coherence pathways are eliminated in each scan, yielding improved digitizer resolution as the receiver gain can be increased to observe the small signals alone. However, standard techniques often incur a sensitivity loss if the desired signal component is not modulated uniformly over the sample volume but instead integrates to a dc level less than unity.

RF-gradient techniques rely on variations in the B_1 field strength to dephase unwanted magnetization components in a plane containing the z axis, in contrast to the transverse phase modulation caused by B_0 gradients. B_1 gradient techniques have a number of intrinsic advantages. The gradients are frequency selective, they may be implemented with standard RF probe and amplifier hardware, they have rapid switching times, and they do not perturb the lock system or require recovery from eddy-current effects.

Most importantly, for some applications, as in the sequences described below, B_1 gradients fit more logically into the pulse sequence structure than B_0 gradients by preserving its overall structure and symmetries. Since RF gradients are capable of simultaneously producing coherence transformations and encoding spatial modulations, they may be incorporated into an experiment without even altering the form of the pulse sequence simply by replacing appropriate excitation pulses with RF gradient pulses. Previous applications of B_1 gradients include solvent suppression (*2, 3*), P/N-type selection (*4, 5*), multiple-quantum filters (*6–8*), and heteronuclear correlation spectroscopy (*9*).

The RF-gradient sequence presented in this report was developed to perform selective excitation and saturation simultaneously, as a function of the scalar coupling constant

‡ To whom correspondence should be addressed, at 150 Albany Street, Room NW14-4110, Cambridge, MA 02139.

1090-7807/97 $25.00

J_{CH}. It is designed so that RF gradients selectively dephase the unwanted magnetization components (here, uncoupled spins with $J = 0$) over the sample volume, while the desired components—those coupled with a particular scalar-coupling strength—are completely refocused. The sequence acts as a selective filter to pass magnetization with a particular scalar-coupling constant. It may be used alone or at any point in a lengthier sequence. It simultaneously eliminates the unwanted signal components while retaining the desired magnetization with no theoretical attenuation factor, in contrast to static B_0 gradient techniques which often sacrifice sensitivity due to signal averaging over the sample volume. It is performed as a single-shot experiment which at the same time makes maximal use of the receiver dynamic range, in contrast to phase-cycling schemes which require the addition of multiple signals of which the desired component is only a small part. A B_0-gradient modification of the BIRD sequence with similar goals has previously been reported (*10*). Like the B_1-gradient version presented here, it dephases unwanted magnetization while retaining the coupled magnetization without any loss in sensitivity.

The effect of the RF-gradient sequence was confirmed here, using only the residual RF inhomogeneity of a standard ''homogeneous'' coil. Practical application of these techniques is likely to benefit further from the use of specially designed RF-gradient coils with an enhanced B_1 inhomogeneity, like those described in (*4, 11*).

BACKGROUND

Building Blocks

Two common pulse-sequence building blocks will be of use in describing the standard BIRD and TANGO sequences as well as their RF-gradient counterparts. The unit $\tau - \pi_x - \tau$ is used in many NMR sequences to refocus evolution under the chemical shift and heteronuclear J couplings. Transverse magnetization acquires a phase $\Delta\omega\tau$ after evolution for time τ under the chemical-shift Hamiltonian $\Delta\omega I_z$. The π pulse inverts this phase angle, resulting in complete refocusing after evolution during the second τ period. Since the π pulse has no effect on the spin state S_z of the heteronuclear coupling partner, the scalar-coupling evolution frequency $2\pi JS_z$ remains the same on both sides of the π pulse, in analogy with the chemical shift, so its effects are refocused as well. The building block thus behaves as π_x while completely refocusing evolution under the chemical shift and the heteronuclear J_{CH} coupling.

The sequence $\tau - \pi_x(^1\text{H}, ^{13}\text{C}) - \tau$ refocuses chemical-shift evolution just as the $\tau - \pi_x(^1\text{H}) - \tau$ unit does. However, the additional π pulse on the X nucleus (here ^{13}C) inverts S_z, reversing the sense of evolution at the same time as the phase inversion. Evolution under the heteronuclear J_{CH} coupling therefore accumulates for both τ periods, as may be seen in the graphical representation of Fig. 1 or in the corresponding product operator description

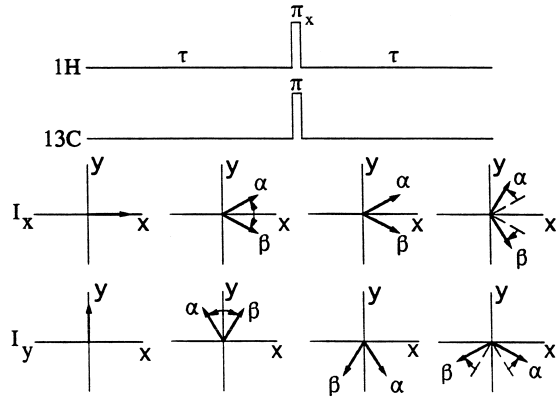

FIG. 1. A common pulse-sequence building block responsible for the selectivity of the standard BIRD and TANGO sequences and their RF-gradient modifications. The sequence is displayed above a graphical representation of the magnetization state at subsequent stages of the pulse sequence. The starting spin state I_x or I_y evolves for a time τ under the chemical-shift Hamiltonian and under a heteronuclear J coupling. Inverting pulses are applied on both nuclei, after which an additional τ evolution occurs resulting in the final spin state. The ^{1}H π_x pulse refocuses evolution under the chemical shift and inverts the ^{1}H spin states about the x axis. The ^{13}C π pulse swaps the ^{13}C spin labels $\alpha \leftrightarrow \beta$ at the same time as the ^{1}H inversion, thus allowing continued evolution under the heteronuclear J_{CH} coupling for the full 2τ period. For $J = 0$, the overall effect is a π_x rotation, while for $J = 1/2\tau$, the net result is π_y.

$$\begin{Bmatrix} I_x \\ I_y \\ I_z \end{Bmatrix} \xrightarrow{\tau} \begin{Bmatrix} I_x\cos(\pi J\tau) + 2I_yS_z\sin(\pi J\tau) \\ I_y\cos(\pi J\tau) - 2I_xS_z\sin(\pi J\tau) \\ I_z \end{Bmatrix}$$

$$\xrightarrow[(^1\text{H}, ^{13}\text{C})]{\pi_x} \begin{Bmatrix} I_x\cos(\pi J\tau) + 2I_yS_z\sin(\pi J\tau) \\ -I_y\cos(\pi J\tau) + 2I_xS_z\sin(\pi J\tau) \\ -I_z \end{Bmatrix}$$

$$\xrightarrow{\tau} \begin{Bmatrix} I_x\cos[\pi J(2\tau)] + 2I_yS_z\sin[\pi J(2\tau)] \\ -I_y\cos[\pi J(2\tau)] + 2I_xS_z\sin[\pi J(2\tau)] \\ -I_z \end{Bmatrix}. \quad [1]$$

This unit behaves as π_x for $J = 0$, and as π_y for $J_{CH} = 1/2\tau$. It is precisely this differential effect on coupled versus uncoupled spins that makes possible the selectivity of the excitation techniques described below. Changing the phase of the central proton π_x pulse to π_y reverses the effect of the building block: the sequence then behaves as a net π_y for uncoupled spins and as π_x for spins coupled with $J_{CH} = 1/2\tau$. All sequences which exert their selective effects through the $\tau - \pi(^1\text{H}, ^{13}\text{C}) - \tau$ building block thus have their actions on coupled versus uncoupled spins reversed by a 90° phase shift of the central proton π pulse.

Standard BIRD Sequence

The standard BIRD$_x$ sequence $(\pi/2)_x - \tau - \pi_x(^1\text{H}, ^{13}\text{C}) - \tau - (\pi/2)_x$ is composed simply of the $\tau - \pi(^1\text{H},$

$^{13}C)-\tau$ unit of Fig. 1 surrounded by $(\pi/2)_x$ pulses (*12*). Replacing the central building block with π_x or π_y for uncoupled and coupled spins, respectively, reveals the behavior of the overall sequence

$$\begin{aligned} J = 0\text{: } (\pi/2)_x\text{—}\overbrace{\tau\text{—}\pi_x(^1\text{H, }^{13}\text{C})\text{—}\tau}^{\pi_x}\text{—}(\pi/2)_x &= 2\pi_x \\ 2J\tau = 1\text{: } (\pi/2)_x\text{—}\underbrace{\tau\text{—}\pi_x(^1\text{H, }^{13}\text{C})\text{—}\tau}_{\pi_y}\text{—}(\pi/2)_x &= \pi_y. \end{aligned} \quad [2]$$

BIRD_x thus acts as a $2\pi_x$ pulse for uncoupled spins and as π_y for coupled magnetization. If the system starts in equilibrium, BIRD_x inverts the coupled magnetization to $-z$ while leaving uncoupled spins along $+z$.

Standard TANGO Sequence

The standard TANGO sequence $(\pi/2 + \alpha)_x\text{—}\tau\text{—}\pi_x(^1\text{H, }^{13}\text{C})\text{—}\tau\text{—}(\pi/2 - \alpha)_x$ can be understood most generally by recognizing its equivalence to the sequence $\alpha_x\text{—}\text{BIRD}_x\text{—}\alpha_{-x}$, simply a formal rotation of the BIRD_x sequence by an angle $-\alpha$ about the x axis (*13*). TANGO thus still acts as a $2\pi_x$ rotation for $J = 0$, leaving uncoupled spins along $+z$. For $2J\tau = 1$, however, the net effect is $\alpha_x\text{—}\pi_y\text{—}\alpha_{-x}$, equivalent to a π rotation about an axis in the y–z plane, at an angle α below the y axis. For the standard TANGO sequence where $\alpha = \pi/4$, coupled magnetization starting along $+z$ is thus placed along $-y$ for $2J\tau = 1$.

RF Gradients

Both the BIRD and TANGO sequences are ideal candidates for RF gradient use. Unlike B_0 gradients which dephase magnetization in the transverse plane, RF gradients spread out magnetization over a plane which is normal to the local B_1 field and which thus contains the z axis. Standard NMR probes are designed to have uniform B_1 profiles, in order to produce uniform excitation and detection profiles across the sample volume, with the object of achieving maximal sensitivity and location-independent effects of multiple-pulse cycles. Even in these probes, however, residual RF inhomogeneity produces differential nutation angles relative to the nominal flip angle. Figure 2 is the result of a nutation experiment for the proton coil from a commercial Bruker 500 MHz $\{^1\text{H, }^{13}\text{C, }^{15}\text{N}\}$ probe. In this experiment, a series of short RF pulses are applied on resonance with one data point collected after each pulse. In order to satisfy the Nyquist condition, the nutation angle of each pulse must be less than π. For an RF axis along x, the net magnetization vector nutates periodically in the y–z plane, but attenuates due to differential nutation of spin packets located in regions of differing RF field strength. The transverse magnetization is thus sine modulated at the RF-nutation frequency ω_1, so

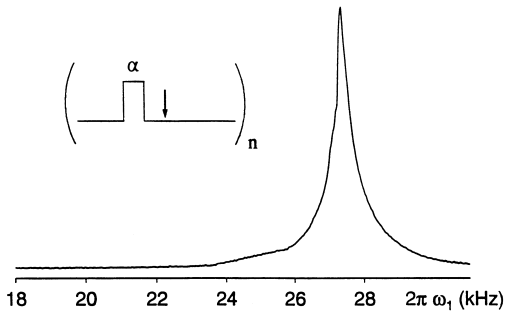

FIG. 2. Nutation experiment: On-resonance RF pulses are applied sequentially to a sample of H_2O, with one data point collected after each pulse. The net magnetization vector nutates about the RF axis at the average ω_1 frequency and attenuates due to the dispersion in RF field strength over the sample volume. Each spin packet contributes a transverse magnetization component that is sine modulated at the local nutation frequency. Fourier transformation then yields the distribution of B_1 field strengths over the sample volume.

Fourier transformation yields the distribution of ω_1 over the sample volume or equivalently, how many spins in the sample experience each particular B_1 field strength. The distribution is highly peaked at the nominal nutation frequency, with a full width at half maximum that is only a few percent of the peak B_1, but it also contains relatively broad shoulders as a significant portion of the sample experiences an RF field that varies from the average value by 5 to 10%.

If a commercial probe with a ''homogeneous'' coil of the sort used in the nutation experiment of Fig. 2 is employed for RF gradient applications, effective averaging requires that long, high-power pulses be used to produce an average nutation many times the nominal 2π pulse length. A coil with a residual RF inhomogeneity of approximately 10%, for example, would spread the magnetization approximately 10 times about the RF axis during a hard pulse whose nominal flip angle is 100 full cycles. This will cause a substantial suppression, but will nonetheless leave some residual net magnetization if spins are not spread uniformly throughout the plane. The exact amount of uncancelled magnetization depends on the geometries of the sample volume and of the RF field inhomogeneity, which determine the shape of the nutation spectrum. The decay envelope during a long RF pulse is simply the inverse Fourier transform of the nutation distribution. Equivalently, as a long RF pulse is applied, one may envision the residual signal as the integral of the nutation spectrum of Fig. 2 after multiplication by a sine function whose pitch increases steadily with time. This sine function represents the differential nutation angle between spin packets sitting in different RF field strengths. For a coil with an inhomogeneity of 10%, 5 periods of the sine wave would fit inside the nutation spectrum after 50 nominal 2π cycles, and 10 periods after 100 cycles. Longer gradient pulses produce more rapidly varying sine modulations and better suppression factors after integration over the ω_1 axis.

This integration over the nutation spectrum in fact occurs

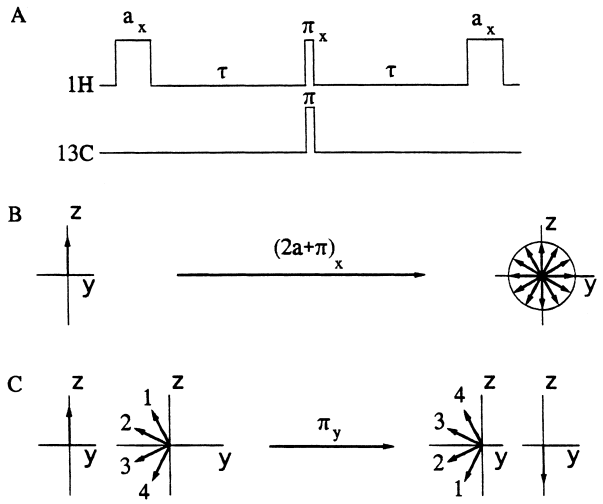

FIG. 3. (A) rBIRD$_x$, the RF-gradient version of the BIRD sequence formed by replacing the $(\pi/2)_x$ pulses of the standard BIRD sequence with RF gradient pulses of spatially varying nutation angle a_x. (B) Uncoupled magnetization with $J = 0$ undergoes a spatially varying RF nutation of angle $(\pi + 2a)_x$ and is thus spread uniformly throughout the $Y-Z$ plane, yielding zero net signal. The vector diagrams schematize the spin states before the first gradient pulse and after the second gradient. (C) Coupled magnetization with $2J\tau = 1$ is refocused in a rotary echo and is entirely recovered. Spin packets 1–4 are located in regions of different RF field strengths and thus undergo different nutation angles a, yet they are all refocused together along the $-z$ axis at the end of the sequence. The spin-packet orientations are shown before and after each gradient pulse.

separately for spin packets at each chemical-shift value. Each of these spin packets must experience sufficient dispersion in ω_1 over the sample volume to produce adequate suppression at each offset. A well-shimmed sample assists the suppression by increasing the spatial spread of each spin packet over sample regions of different RF field strength.

For the experiments described below, long RF pulses were used as RF-gradient pulses, utilizing the slight B_1 inhomogeneity to produce effective dephasing. Homogeneous pulses of short duration were used to produce the standard $\pi/2$ and π pulses.

RF GRADIENT SEQUENCES

Without further complication of the sequences, BIRD and TANGO can be modified to eliminate the uncoupled magnetization rather than leaving it unperturbed along $+z$. At the same time, these modified sequences result in complete retention of the desired magnetization that is directly bound to a coupling partner with a scalar coupling constant $J_{CH} = 1/2\tau$.

RF Gradient BIRD (rBIRD)

The RF gradient BIRD sequence is formed simply by replacing the $(\pi/2)_x$ pulses in the standard sequence with long RF-gradient pulses a_x which result in nutation angles a that vary throughout the sample in a manner dependent on the coil geometry. This sequence is depicted in Fig. 3A.

The first RF gradient pulse dephases all magnetization components in the $y-z$ plane. The central $\tau-\pi(^1H, ^{13}C)-\tau$ unit is then the key to the sequence's selective action on coupled versus uncoupled magnetization. For $J = 0$, the central building block unit results in a π_x nutation about the RF axis. The second gradient pulse then causes further dephasing. The result is that uncoupled magnetization nutates through a spatially dependent angle $(\pi + 2a)_x$ and is spread throughout the $y-z$ plane (Fig. 3B). For a sufficiently long RF gradient pulse, a varies continuously over many cycles throughout the range zero to 2π and the net signal integrates to zero:

$$J = 0\text{: } I_z \Rightarrow \int_0^{2\pi} [-I_z\cos(2a) + I_y\sin(2a)]da = 0$$

$$2J\tau = 1\text{: } a_x - \pi_y - a_x = a_x - \underbrace{\pi_y - a_x - \pi_{-y}}_{a_{-x}} - \pi_y = \pi_y. \quad [3]$$

For $2J\tau = 1$, however, the effect of the central unit is instead a π_y rotation, which causes the second gradient pulse to refocus the magnetization completely in a rotary echo and results in complete retention of this magnetization component (Fig. 3C). Substituting the equivalent rotation a_{-x} for $\pi_y-a_x-\pi_{-y}$ in Eq. [3] makes it clear that the net effect on coupled magnetization is simply a net π_y rotation.

Alternatively, the experiment is easily described by requantizing the spin states along the axis of the RF-gradient pulses (*14*). Any magnetization—transverse or longitudinal—that is in a plane orthogonal to the RF axis may be viewed as a combination of states with effective coherence numbers $k_x = \pm 1$ when quantized along the RF axis (here along x). These states thus dephase in the RF gradient, just as z-quantized ± 1 quantum coherences dephase about the z axis under the influence of a B_0 gradient. Conversely, transverse magnetization that lies along the RF axis has an effective coherence number of $k_x = 0$ in this basis set and does not therefore evolve during the gradient pulse. For uncoupled magnetization, the sequence acts simply as a single gradient pulse, dephasing the starting states (I_z and I_y) with $k_x = \pm 1$, while preserving the spin-locked state (I_x) with $k_x = 0$. For the coupled magnetization, however, the action of the central $\tau-\pi_x-\tau$ unit as π_y inverts the effective coherence numbers $k_x = \pm 1$ to $k_x = \mp 1$, causing evolution in the opposite sense during the second gradient pulse, and resulting in complete refocusing. The spin dynamics are thus analogous to those of a B_0 gradient echo sequence $G-\pi-G$, once the spin states have been requantized along the appropriate gradient evolution axis.

RF Gradient TANGO

An RF-gradient version of the TANGO sequence can likewise be created to eliminate uncoupled magnetization while

TABLE 1
Comparison of Error Terms for the Standard and RF-Gradient BIRD Sequences

Source of error		$BIRD_x$		$rBIRD_x$
Incorrect τ	I_z	$I_x \cos[\pi J(2\tau)] + 2I_zS_z \sin[\pi J(2\tau)]$	I_x	$I_x \cos[\pi J(2\tau)]$
	$I_y \Rightarrow$	I_y	$I_y \Rightarrow$	$I_y \sin^2[\pi J\tau]$
	I_z	$I_z \cos[\pi J(2\tau)] + 2I_xS_z \sin[\pi J(2\tau)]$	I_z	$-I_z \sin^2[\pi J\tau]$
Incorrect length of π (^{13}C): pulse length ($\pi + \epsilon$), $2J\tau = 1$	I_x	$-I_x \cos(\epsilon) - 2I_zS_z \sin(\epsilon)$	I_x	$-I_x \cos(\epsilon)$
	$I_y \Rightarrow$	I_y	$I_y \Rightarrow$	$I_y \cos^2(\epsilon/2)$
	I_z	$-I_z \cos(\epsilon) + 2I_xS_z \sin(\epsilon)$	I_z	$-I_z \cos^2(\epsilon/2)$
Incorrect length of π_x (^{1}H): pulse length ($\pi + \epsilon$), $\Delta\omega = 0$, $2J\tau = 1$	I_x	$-I_x\cos(\epsilon) - 2I_yS_z \sin(\epsilon)$	I_x	$-I_x \cos(\epsilon)$
	$I_y \Rightarrow$	$I_y \cos(\epsilon) - 2I_xS_z \sin(\epsilon)$	$I_y \Rightarrow$	$I_y \cos^2(\epsilon/2)$
	I_z	$-I_z$	I_z	$-I_z \cos^2(\epsilon/2)$

placing coupled spins in the transverse plane. In analogy with the standard sequence, the RF-gradient version is formed simply as α_x—$rBIRD_x$—α_{-x}. As the a_x pulses in the central rBIRD unit are long RF-gradient pulses causing complete dephasing, they may be arbitrarily lengthened by α_x to yield $rBIRD_x$—$2\alpha_{-x}$, which is identical to the rBIRD sequence of Fig. 3A followed by a $2\alpha_{-x}$ pulse to nutate the refocused magnetization from $-z$ into the transverse plane. The rBIRD component eliminates the uncoupled magnetization while placing coupled spins along $-z$, which are then caused to nutate into the transverse plane by the additional 2α rotation. For $\alpha = \pi/4$, the magnetization with $2J\tau = 1$ is placed along $-y$, as in the standard sequence. The difference between the standard sequence and the RF-gradient modification is once again the elimination of the unwanted signal component with $J = 0$.

Miscalibration Error Terms

The standard BIRD and TANGO sequences are typically rather sensitive to incorrectly set pulse lengths and delays, which result in error terms that are antiphase or that may be transformed into antiphase states (and other multiple quantum coherences) by later RF pulses. The RF-gradient version, on the other hand, is relatively forgiving of incorrectly set experimental parameters. Misset delays or pulse lengths result purely in attenuation of the desired terms, but do not create any multiple-quantum coherences. The ability to excite coherence transformations while simultaneously removing troublesome signal components is a property unique to RF gradients, which further supports their utility as the most natural means of selective excitation in this and other related pulse sequences. The error terms arising from a variety of miscalibrations are straightforward to calculate with the product-operator formalism. Table 1 compares the transformations between spin states that occur with the standard $BIRD_x$ sequence and the RF-gradient $rBIRD_x$ modification.

To review, both sequences provide complete retention of the directly coupled magnetization components with $2J\tau = 1$, acting merely as a net π_y rotation to invert I_x and I_z with no effect on I_y. $\{I_x, I_y, I_z\}$ should thus transform to $\{-I_x, I_y, -I_z\}$. Conversely, for uncoupled magnetization with $J = 0$, the $BIRD_x$ sequence acts as $2\pi_x$, leaving all components in their starting state, while the RF-gradient version $rBIRD_x$ performs spin-locking about the x axis, completely eliminating all spin states not aligned along x.

The first row of the table presents the error terms arising from an incorrectly set evolution delay τ. Equivalently, it demonstrates the sensitivity of both sequences to the coupling strength J. If τ is set incorrectly for the system of interest, or, as is commonly the case, the sample contains coupled partners with a range of coupling constants J, complete preservation of the coupled magnetization does not occur. The standard $BIRD_x$ sequence produces zero-quantum and antiphase error terms, which are eliminated by the RF-gradient version. Furthermore, for a starting I_z spin state, the rBIRD sequence retains the desired final $-I_z$ component with higher efficiency, varying with the coupling constant J as $\sin^2(\pi J\tau)$ rather than as $\cos(2\pi J\tau)$. For small miscalibrations $2J\tau = 1 - \epsilon/\pi$, the retention efficiency of rBIRD decreases at half the rate of the standard sequence, varying as $1 - \epsilon^2$ rather than $1 - 2\epsilon^2$.

The second and third rows, respectively, demonstrate the error terms that arise from miscalibration of the carbon π pulse and the proton π pulse, performed on resonance for magnetization coupled with $2J\tau = 1$. The standard sequence again produces zero- and single-quantum error terms, which are again eliminated by the RF-gradient technique, at the cost of a slight attenuation. The BIRD (or TANGO) sequence is commonly used to perform selective excitation of desired coupling partners as a first step in longer experiments. While it is possible to use phase cycling or gradient techniques to remove the miscalibration error terms that can be converted into undesired coherences by later pulses, the intrinsic elimination of these imperfections by the RF-gradient sequence is of advantage experimentally.

EXPERIMENTAL RESULTS

Figure 4 shows experimental spectra of a chloroform sample, obtained on a Bruker 500 MHz Avance DRX spectrome-

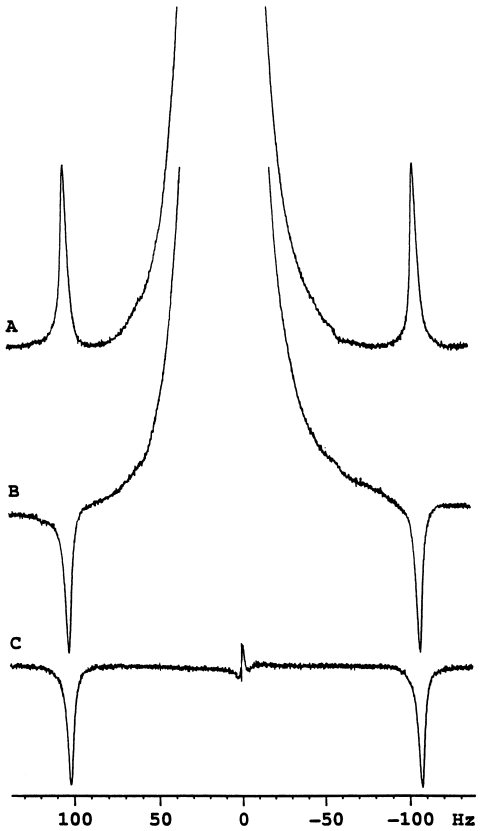

FIG. 4. A sample of 10% $CHCl_3$ in $CDCl_3$ was used to investigate the RF-gradient BIRD sequence (rBIRD) on a Bruker 500 MHz DRX spectrometer. Chromium acetylacetonate (CrAcAc) was added to reduce T_1 to 4 s. (A) Chloroform spectrum, expanded to show the satellites; (B) the standard $BIRD_x$ sequence, showing satellite inversion; (C) the result of $rBIRD_x$—$rBIRD_x$—$(\pi/2)_x$, demonstrating significant suppression of the central peak with 80% refocusing of the satellites, as compared with (B). The RF-gradient pulses had duration $\alpha_x = 4.5$ ms, and the $\pi/2$ pulse duration was 9 μs. All three sequences were performed on resonance. (B) and (C) use $\tau = 2.38$ ms, corresponding to $J_{CH} = 210$ Hz.

ter, using the probe whose nutation spectrum was shown in Fig. 2. The proton spectrum of chloroform in Fig. 4A reveals a large uncoupled central line that arises from protons bound to the nonmagnetic ^{12}C nuclei. This peak is flanked by the ^{13}C-bound satellites, which are 200 times smaller than the uncoupled line, since ^{13}C has a natural abundance of only 1% (0.5% in each satellite). Figure 4B shows the results of the standard BIRD sequence, followed by $\pi/2$, which selectively inverts the satellites without affecting the uncoupled magnetization. Figure 4C demonstrates that the RF-gradient BIRD sequence then yields substantial suppression of the uncoupled magnetization—by a factor of approximately 800—reducing its magnitude to well below that of the satellites, which are refocused to a magnitude that is 80% that of Fig. 4B. The rBIRD sequence of Fig. 3A was repeated twice with the same RF phase in order to reduce attenuation of the desired magnetization due to molecular diffusion and to ease the demands placed on the RF amplifier as explained below in the discussion. It was then followed by a $\pi/2$ pulse to place the satellites in the transverse plane. The nominal nutation caused by all four RF-gradient pulses was 500 complete cycles, resulting in substantial suppression due to the coil's residual B_1 inhomogeneity.

DISCUSSION

While the RF-gradient sequence causes substantial suppression after a single-shot experiment, residual uncoupled magnetization does survive the sequence as a result of imperfect dephasing by the RF gradients. Conversely, not all of the magnetization with the correct coupling strength $2J\tau = 1$ is refocused. There are several experimental factors responsible for both the incomplete suppression and the imperfect refocusing.

Imperfect refocusing of coupled magnetization occurs primarily as a result of molecular diffusion in those regions of the sample where the local RF gradient is strongest. During the 2τ delay between the RF-gradient pulses, and during the gradient pulses themselves, diffusion causes molecular displacements to nearby regions of different B_1 field strength, which results in incomplete refocusing by the second gradient pulse. If the RF gradient were linear, the diffusive attenuation factor during this sequence would be the same as that of a standard pulsed-gradient spin-echo (PGSE) diffusion experiment using a static B_0 gradient (*15*). Linear RF gradients have in fact been used successfully in diffusion experiments by making use of this correspondence (*11*). For the RF-gradient BIRD sequence, the predicted attenuation factor is thus

$$A = \exp\{-(\gamma g \delta)^2 D(2\tau + 2\delta/3)\}, \qquad [4]$$

where D is the diffusion constant, δ is the length of each linear gradient pulse, and 2τ is the separation between the defocusing and refocusing gradient pulses. However, since the RF gradients are not linear across the sample in the coil used in this work, this attenuation factor does not apply globally across the entire sample but must be summed over local regions of different RF-gradient strength. Greater attenuation occurs in sample regions experiencing a stronger gradient. Nonetheless, solving for g in Eq. [4] with $D = 2.4$ $\mu m^2/ms$ for chloroform, and with the observed signal amplitude of 88% for $\delta = 4.5$ ms and $\tau = 2.4$ ms, yields an effective linear-gradient strength of approximately 7 G/cm, which corresponds to a variation in nutation frequency of 30 kHz/cm. The central sample regions, where the RF field is most uniform, contribute very little to the attenuation, while those regions near the top and bottom of the coil experience a much higher RF gradient and thus attenuate more rapidly.

For the coil used here, with a nominal nutation frequency of 27 kHz, a B_1 gradient larger than 7 G/cm can reasonably be expected over a large enough fraction of the sample to

account for the observed attenuations: Two-dimensional nutation experiments (nutation frequency vs z position) reveal that near the ends of a 5 mm diameter, 1 cm long homogeneous coil, the nutation frequency falls rapidly from near maximum to near zero over a distance of only a couple millimeters. While this diffusive attenuation is noticeable for a rapidly diffusing molecule such as chloroform, it would be much less significant for larger molecules which diffuse more slowly, which would thus refocus more completely.

The residual uncoupled signal that survives the RF-gradient BIRD sequence is due primarily to incomplete averaging by the RF gradients. As discussed above, the inverse Fourier transform of the coil's nutation spectrum yields the expected decay envelope of uncoupled magnetization as a function of the RF-gradient pulse length. To achieve better averaging, one must either apply longer RF-gradient pulses, repeat the experiment serially, or use an RF coil with a larger B_1 inhomogeneity.

While it is possible to increase the RF gradient pulse lengths, the long, high-power pulses required when using a homogeneous coil do pose some experimental challenges. The frequency selectivity of long RF pulses could limit the spectral width over which suppression is effective. RF power deposition in the sample may also be of concern for certain samples. The most significant issues, however, depend upon the probe and RF amplifier used. During the pulse, an RF-phase shift or a gradual decline in the power output of the RF amplifier may appear. Alternatively, heating of the probe may occur, thus altering the probe's Q factor which may cause variations in the phase or intensity of the RF transmitted to the sample. These RF amplitude and phase effects may be corrected by adjusting the lengths and phases of the refocusing gradient pulses. For the hardware used here, the dominant effect was a slight droop in the amplifier output, easily corrected by lengthening the second gradient pulse (by about 1%).

As an alternative to the long-pulse approach, it is possible instead to use shorter RF-gradient pulses while repeating the sequence twice or more in series, thus producing further dephasing of the uncoupled magnetization with each repetition. This approach decreases the average RF duty cycle, potentially easing several of the difficulties associated with long RF pulse lengths. Furthermore, as the desired magnetization component is refocused at the end of each repetition, losses due to molecular diffusion are reduced, just as diffusive attenuation factors can be reduced with a Carr–Purcell cycle. This is indeed observed experimentally—a single rBIRD sequence with 9 ms gradient pulses refocuses only 62% of the desired signal, while two serial repetitions using 4.5 ms pulses yield nearly 80% refocusing (close to the square of the 88% factor from a single repetition using 4.5 ms gradients). For additive suppression effects, the sequence must be applied with the same RF phase during subsequent repetitions. Shifting the RF phase by 90° during a second repetition causes only half of the original uncoupled magnetization to dephase further, while the other half is instead refocused.

Finally, suppression factors may be improved by using a probe with an RF-gradient coil specifically designed with enhanced B_1 inhomogeneity to produce better averaging over the sample volume (*4, 11*). This broadens the nutation spectrum, producing superior dephasing with shorter RF-gradient pulses, and thus eliminates the pulse duration issues discussed above. Sequences employing RF gradients typically require homogeneous pulses as well as the gradient pulses to retain sensitivity. The rBIRD sequence, for example, requires fairly homogeneous π pulses to achieve full refocusing. As a result, RF-gradient probes typically contain both a homogeneous coil and a gradient coil, either with separate RF amplifiers for each coil (*11*) or with active switching between the two coils (*4*).

When RF-gradient techniques are performed over a range of resonance offsets, it is difficult to achieve uniformly excellent suppression factors. This occurs because a portion of the starting magnetization is spin locked due to the slight tilt of the effective RF axis out of the transverse plane. The RF gradient dephases only the magnetization component that is orthogonal to the RF axis while spin locking the parallel component. The tilt of the effective RF axis from the transverse plane is $\theta = \tan^{-1}(\Delta\omega/\omega_1)$. The residual spin-locked fraction is simply the projection of the starting magnetization vector onto the RF axis and is thus equal to $\tan(\theta) = \Delta\omega/\omega_1$. This accurately predicts the observed magnitude of the spin-locked magnetization, corresponding to $\approx$2% of the magnetization at an offset of 500 Hz for the RF coil used here with an average $\omega_1 \approx 27$ kHz. When applying the RF-gradient sequence off resonance, as for a sample spanning a large spectral width, this spin-locked component must therefore be eliminated. The rBIRD$_x$ sequence may be followed by a $(\pi/2)_{-y}$ pulse to nutate the spin-locked component from the x axis back to $-z$, although this approach leaves net uncoupled magnetization which may be significant if later manipulations are planned. This residual magnetization may instead be eliminated by incorporating a two-step phase cycle which adds the results of rBIRD$_x$—$(\pi/2)_y$ and rBIRD$_{-x}$—$(\pi/2)_y$. Alternatively, the usual $(\pi/2)_x$ pulse may be applied, followed by a brief RF-gradient pulse along y to dephase the previously spin-locked component while spin locking the coupled magnetization component. This requires that the orthogonal y-gradient pulse be made short compared to the total preceding RF-gradient length in order to avoid refocusing half the magnetization.

The other approach to avoid spin locking is to place the starting spin state orthogonal to the tilted effective RF axis. A composite pulse (*16*) compensated for resonance offset could be used to nutate the starting I_z state to I_y before applying the gradient sequence with an RF phase of x. A different, elegant solution was presented by Canet *et al.* (*17*), in which the first gradient pulse is preceded by $(\pi/2)_x$—τ—$(\pi/2)_{-x}$. During the τ interval, chemical-shift

evolution occurs, so for small offsets $\Delta\omega \ll \omega_1$, the sequence may be represented as $(\pi/2)_x$—$(\Delta\omega\tau)_z$—$(\pi/2)_{-x}$ = $(-\Delta\omega\tau)_y$. By choosing $\tau = 1/\omega_1$, the magnetization vector then nutates to a position tilted by $-\Delta\omega/\omega_1 \approx -\theta$ from the z axis, orthogonal to the effective RF axis of the gradient pulse that follows. More complete dephasing thus occurs over a larger range of offsets.

CONCLUSIONS

By combining the steps of coherence-pathway transformation and spatial modulation, RF gradients are ideally suited for certain types of selective-excitation sequences, such as the RF-gradient BIRD/TANGO sequence presented here. The incorporation of RF gradients may be achieved without altering the form of the pulse sequence, while at the same time eliminating not only the target magnetization component (here the uncoupled magnetization with $J = 0$) but also a variety of coherences that normally arise from imperfectly set pulse lengths and evolution delays. RF gradients pose a variety of experimental challenges—especially when using the residual B_1 inhomogeneity of a nominally homogeneous coil. Nonetheless, rBIRD is capable of producing substantial suppression factors in eliminating uncoupled magnetization, as predicted by theory. General application of these techniques would ideally employ specially designed RF-gradient coils to provide more complete elimination of unwanted magnetization components while at the same time alleviating experimental challenges associated with the use of long high-power RF-gradient pulses.

ACKNOWLEDGMENTS

The authors thank Dr. W. E. Maas for helpful discussions. This work was funded in part by the National Institute for Health (R01-GM52026-01, RR-00995) and the National Science Foundation (DMR-9357603).

REFERENCES

1. J. Keeler, R. T. Clowes, A. L. Davis, and E. D. Lowe, *Methods Enzymol.* **239,** 145–207 (1994).
2. D. Canet, J. Brondeau, E. Mischler, and F. Humbert, *J. Magn. Reson. A* **105,** 239–244 (1993).
3. W. E. Maas and D. G. Cory, *J. Magn. Reson. A* **106,** 256–259 (1994).
4. D. G. Cory, F. H. Laukien, and W. E. Maas, *J. Magn. Reson. A* **103,** 115–117 (1993).
5. P. Mutzenhardt, J. Brondeau, and D. Canet, *J. Magn. Reson. A* **108,** 110–115 (1994).
6. C. J. R. Counsell, M. H. Levitt, and R. R. Ernst, *J. Magn. Reson.* **64,** 470–478 (1985).
7. J. Brondeau, D. Boudot, P. Mutzenhardt, and D. Canet, *J. Magn. Reson.* **100,** 611–618 (1992).
8. D. G. Cory, F. H. Laukien, and W. E. Maas, *J. Magn. Reson. A* **105,** 223–229 (1993).
9. W. E. Maas and D. G. Cory, *J. Magn. Reson. A* **112,** 229–236 (1995).
10. C. Emetarom, T. Hwang, G. Mackin, and A. J. Shaka, *J. Magn. Reson. A* **115,** 137–140 (1995).
11. D. Canet, B. Diter, A. Belmajdoub, J. Brondeau, J. C. Boubel, and K. Elbayed, *J. Magn. Reson.* **81,** 1–12 (1989).
12. J. R. Garbow, D. P. Weitekamp, and A. Pines, *Chem. Phys. Lett.* **93,** 504–509 (1982).
13. S. C. Wimperis and R. Freeman, *J. Magn. Reson.* **58,** 348–353 (1984).
14. Y. Zhang, W. E. Maas, and D. G. Cory, *Mol. Phys.* **86,** 347–358 (1995).
15. E. O. Stejskal, and J. E. Tanner, *J. Chem. Phys.* **42,** 288–299 (1965).
16. M. H. Levitt, *Prog. NMR Spectrosc.* **18,** 61–122 (1986).
17. P. Mutzenhardt, J. Brondeau, and D. Canet, *J. Magn. Reson. A* **117,** 278–284 (1995).